BIOCHEMISTRY
including biophysical chemistry & molecular biology

Article

pubs.acs.org/biochemistry

Probing Ligand Binding to Thromboxane Synthase

Wei-Chih Chao,[†] Jyh-Feng Lu,[†] Jinn-Shyan Wang,*[,†] Hsiao-Ching Yang,[‡] Tai-An Pan,[‡] Steven Chun-Wei Chou,[§] Lee-Ho Wang,[∥] and Pi-Tai Chou[§]

[†]School of Medicine, Fu-Jen Catholic University, New Taipei, Taiwan, R. O. C.

[‡]Department of Chemistry, Fu-Jen Catholic University, New Taipei, Taiwan, R. O. C.

[§]Department of Chemistry, National Taiwan University, Taipei, Taiwan, R. O. C.

[∥]Division of Hematology, Department of Internal Medicine, The University of Texas Health Science Center at Houston, Houston, Texas 77030, United States

Supporting Information

ABSTRACT: Various fluorescence experiments and computer simulations were utilized to gain further understanding of thromboxane A_2 synthase (TXAS), which catalyzes an isomerization of prostaglandins H_2 to give rise to thromboxane A_2 along with a fragmentation reaction to 12-L-hydroxy-5,8,10-heptadecatrienoic acid and malondialdehyde. In this study, 2-*p*-toluidinylnaphthalene-6-sulfonic acid (TNS) was utilized as a probe to assess the spatial relationship and binding dynamics of ligand−TXAS interactions by steady-state and time-resolved fluorescence spectroscopy. The proximity between TNS and each of the five tryptophan (Trp) residues in TXAS was examined through the fluorescence quenching of Trp by TNS via an energy transfer process. The fluorescence quenching of Trp by TNS was abolished in the W65F mutant, indicating that Trp65 is the major contributor to account for energy transfer with TNS. Furthermore, both competitive binding experiments and the computer-simulated TXAS structure with clotrimazole as a heme ligand strongly suggest that TXAS has a large active site that can simultaneously accommodate TNS and clotrimazole without mutual interaction between TNS and heme. Displacement of TNS by Nile Red, a fluorescence dye sensitive to environmental polarity, indicates that the TNS binding site in TXAS is likely to be hydrophobic. The Phe cluster packing near the binding site of TNS may be involved in facilitating the binding of multiple ligands to the large active site of TXAS.

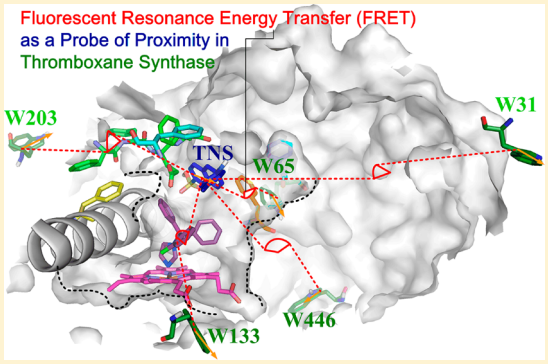

Thromboxane A_2 synthase (TXAS) catalyzes an isomerization of prostaglandins H_2 (PGH_2) to form thromboxane A_2 (TXA_2) but also alternatively performs a fragmentation reaction, producing 12-L-hydroxy-5,8,10-heptadecatrienoic acid (HHT) and malondialdehyde (MDA).[1] TXA_2 is a potent inducer of vasoconstriction and platelet aggregation and has been implicated as an autocrine or a paracrine lipid mediator contributing to a variety of cardiovascular and pulmonary diseases such as atherosclerosis, myocardial infarction, and asthma.[2−4] Because of its unstable epoxy bond, TXA_2 is relatively labile with a half-life of ∼30 s in aqueous solution, hydrolyzing to the biologically inactive thromboxane B_2 (TXB_2) without the need of an enzyme.[5] On the other hand, the biological functions of HHT and MDA are still unclear, although MDA has been shown to participate in the formation of proteins, phospholipids, or DNA adducts that may contribute to the etiology of human diseases.[6,7]

TXAS, a 59 kDa protein, belongs to the cytochrome P450 superfamily.[8,9] Unlike other microsomal P450s that catalyze mono-oxygenation, TXAS catalyzes an isomerization of an endoperoxide and does not need molecular oxygen, reductase, or any other external electron donor. Previous results from UV−visible, magnetic circular dichroism (MCD), and electron paramagnetic resonance (EPR) spectra indicated that recombinant human TXAS has a typical low-spin ferric heme,[10] which is in good agreement with the initial work with TXAS isolated from human platelets.[11] "Truth diagram" analysis of heme EPR revealed that the distal pocket in TXAS is relatively hydrophobic, similar to that in $P450_{cam}$ but distinct from the more polar pockets in chloroperoxidase and nitric oxide synthase.[10] Spectral binding assays showed that TXAS binds strongly to relatively bulky ligands such as clotrimazole and miconazole, indicating that the distal binding domain of heme is spacious. However, the structural information about TXAS is still limited at present because of the lack of X-ray crystallographic structure. Therefore, unraveling the structural−functional relationships of TXAS remains an essential step in understanding the catalytic mechanism of TXAS. Although homology building studies with TXAS using $P450_{BM3}$ as a template have been reported previously,[12,13] it may be necessary to carefully reexamine the three-dimensional (3D) structural model because of their low levels of identity based on

Received: October 15, 2012
Revised: January 15, 2013
Published: January 17, 2013

sequence alignment. Several protein crystal structures have recently been elucidated; the cytochrome P450 3A4 (CYP3A4) heme protein domain showed a significantly high level of sequence identity and homology with TXAS.[14,15] The well-characterized crystallographic data of CYP3A4 are thought to provide the most useful structural information so far for modeling studies with TXAS.

Fluorescence quenching of the indole chromophore has been widely used for a variety of proteins to explore the topological information and hence structurally related properties. This is mainly due to the fact that the fluorescence of the indole chromophore is highly sensitive to the environment.[16−19] To gain a better understanding of the structural−functional relationships of TXAS, we used fluorescence spectroscopy, in combination with systematic site-directed mutagenesis, to probe the TXAS−ligand interaction via the ligand-associated change in the fluorescence property of Trp. In this study, we chose TNS, which has been used as a probe for examining protein−ligand dynamics of CYP3A4, a major enzymatic determinant of drug and xenobiotic metabolism.[20−23] TNS fluoresces weakly at ∼500 nm in aqueous solution and intensely fluoresces at 425−460 nm only when bound to a hydrophobic pocket of a protein. TNS−TXAS binding dynamics was investigated using both steady-state and time-resolved fluorescence spectroscopy. Human TXAS contains five Trp residues; the fluorescence property of Trp in TXAS was used to monitor the accessibility of Trp residues in ligand-bound TXAS and their microenvironment.[24] The results, in combination with systematically mutating Trp sites in TXAS and competitive binding experiments with clotrimazole and Nile Red, provided spectroscopic evidence of the nature of the ligand binding environment of the TXAS as well as identification of the proximity between tryptophan residue(s) and the bound TNS.

MATERIALS AND METHODS

Expression and Purification of Recombinant Human TXAS. Recombinant human TXAS and its mutants were expressed and purified as described by Hsu and Wang[25] with slight modifications. In brief, the constructs were designed by replacing the first 28 amino acid residues in the N-terminal transmembrane domain with the hydrophilic sequence MAKKTSS for TXAS cDNA. A four-histidine tag was added to the C-terminus of TXAS constructs to facilitate protein purification. The expression constructs for the recombinant TXAS proteins carrying single mutations (W31F, W65F, W133F, W203F, and W466F), in which the Trp residues at positions 31, 65, 133, 203, and 466 were individually mutated to phenylalanine (Phe, F), were generated from the TXAS construct mentioned above according to the instructions for the QuikChange site-directed mutagenesis kit (Stratagene).

The expression constructs for the recombinant TXAS protein with multiple mutations were derived from the single-mutant recombinant TXAS constructs either by subcloning using appropriate restriction endonucleases or by site-directed mutagenesis. All constructs were validated by DNA sequencing prior to protein expression. The resulting TXAS cDNAs were transformed into *Escherichia coli* strain BL21/(DE3)pLys for protein expression. Bacterial cultures were grown in 2×YT medium with 50 μg/mL ampicillin (37 °C, 220 rpm) to an OD_{600} of 0.4−0.5. δ-Aminolevulinic acid (δ-ALA, 0.25 mM) was then added to the resulting culture and the culture grown for an additional 30 min prior to the induction of TXAS expression with lactose (∼110 mM; 30 °C for 18−20 h at 200 rpm). The cells were then harvested by centrifugation (6500 rpm for 15 min) and then frozen at −80 °C. To purify recombinant TXAS, the cell pellets were first thawed and then resuspended in sodium phosphate buffer (50 mM, pH 7.5; containing 0.1 M NaCl, 10% glycerol, 10 μg/mL DNase, and 2 mM $MgCl_2$) at a buffer solution:cell pellet ratio of 4:1 (v:w) and then lysed by sonication at 4 °C. TXAS proteins were further solubilized by the addition of NP-40 (3%) with stirring (4 °C, overnight). The TXAS-containing supernatant was collected by centrifugation (4 °C and 30000 rpm) and subjected to purification via a Ni-NTA column (Qiagen) followed by a hydroxyapatite chromatography column to maximize the purity as previously described.[25] The concentration and purity of the resulting TXAS enzymes were determined by the A_{418}/A_{280} ratio, adjusted to 40 μM by dilution with NaP_i buffer (200 mM, pH 7.5; containing 10% glycerol, 0.2% cholic acid, and 0.05% lubrol), and stored at −80 °C. All purified mutant TXASs exhibited a Soret peak at 418 nm similar to that of the wild type in UV−vis spectra.

Optical and Fluorescence Spectroscopy. Absorption studies were performed with a Thermo Evolution 100 UV−vis spectrophotometer (scan rate of 5 nm/s). Fluorescence studies were performed with a Thermo Aminco Bowman Series 2 instrument with a nitrogen lamp (aperture of input and output, 4 nm; scan rate, 5 nm/s). Corrections for the inner filter effect have been made with the following equation[26]

$$F = F_{obs} \times 10^{(A_{ex}+A_{em})/2} \quad (1)$$

where F is the corrected fluorescence intensity and F_{obs} is the background-subtracted fluorescence intensity of the sample. A_{ex} and A_{em} are the measured absorbances at the excitation and emission wavelengths, respectively.

Dissociation constants (K_d) were determined by fitting the data with a one-site saturation ligand binding equation using Sigma Plot version 10.0.

$$F = \frac{F_{max}[S]}{K_d + [S]} \quad (2)$$

The K_d in the inset of Figure 2 was determined by a one-site ligand binding fitting equation expressed as

$$F = F_{max} - (F_{max} - F_{min})\frac{[S]}{K_d + [S]} \quad (3)$$

where F_{max} and F_{min} are the maximal and minimal fluorescence intensity corresponding to ligand concentration [S], respectively.

Nanosecond−microsecond lifetime studies were performed with an Edinburgh FL 900 photon-counting system with a hydrogen-filled lamp as the excitation source. Detailed fluorescence lifetime measurement has been described previously.[27] In brief, nanosecond lifetime studies were performed with an Edinburgh FL 900 photon-counting system with a hydrogen-filled lamp as the excitation source with a 40 kHz repetition rate. The emission decays were analyzed by the sum of exponential functions and convoluted with the instrument response function (IRF), which allowed partial elimination of instrument time broadening and thus rendered a temporal resolution of ∼300 ps.

$$I(t) = \sum_{i=1}^{n} \alpha_i e^{-\tau/\tau_i} \quad (4)$$

Figure 1. Alignment of amino acid sequences of human TXAS and CYP3A4. Analysis of pairwise sequence alignment using the dot matrix method shows a final overall alignment that is 32.7% identical and 57.2% similar between TXAS and P450 3A4.

where τ is the lifetime and α_i is the time zero amplitude due to each decay time (τ_i). To obtain useful structure information from energy transfer, the measured efficiency must be related to the distance between the two fluorophores. FRET efficiency E can be obtained by measuring the fluorescence intensity

$$E = \frac{R_0^6}{R_0^6 + r^6} = 1 - \frac{F_{DA}}{F_D} \quad (5)$$

where F_{DA} is the fluorescence of the donor with the acceptor and F_D is the fluorescence of the donor without the acceptor. Förster distance R_0 can be derived from eq 6.[28]

$$R_0 = \left[\frac{9000(\ln 10)\kappa_p^2 Q_D}{128 N_A \pi^5 n_D^4} I\right]^{1/6} \quad (6)$$

where Q_D is the quantum yield of the donor, N_A is Avogadro's number, and I is the overlap integral between the extinction spectrum of the acceptor and the normalized emission spectrum of the donor. Most investigators assume a random orientation of the donor and acceptor transition dipoles resulting in a value of $^2/_3$ for κ_p^2. In theory, κ_p^2 for any restricted motion can range between 0 and 4, depending upon the orientation. However, it is generally believed that the pocket in TXAS being probed is rather spacious, rendering a high flexibility that may account for the absence of crystal formation for TXAS. On this basis, the assumption of $^2/_3$ for κ_p^2 may be justified. It is worth noting that a value of $^2/_3$ for κ_p^2 has been used frequently in FRET studies of proteins.[29,30] Also, the value for the refractive index of the medium (n_D) is 1.4, which is generally adopted in protein research.

Homology Modeling Structure of Human TXAS. The primary sequence of human TXAS used in this study was obtained from NCBI (GenBank entry AAH41157.1) that was derived from TXAS cDNA containing 1602 nucleotide bases, which is translated to 534 amino acid residues. A search for secondary structures with homology to TXAS was performed using Basic Local Alignment Search Tool (BLAST). The accuracy of the sequence alignment is very important, because the position of the amino acid within the framework depended entirely on this alignment. The similarity between TXAS and the heme protein domain of CYP3A4 covered more than 90% of the TXAS residues. The crystal structure of human microsomal CYP3A4 [Protein Data Bank (PDB) entry 1TQN)] was selected as the template structure for the homology target structure of TXAS. The molecular modeling procedure followed a modification of the strategy developed for other mammalian P450s.[12] Briefly, TXAS was first aligned with the heme protein domain of CYP3A4 based on protein sequence similarity. The conserved helices and strand framework of the CYP3A4 template provided the coordinates for the main chain of TXAS by transferring the crystal structure coordinates of the CYP3A4 template to the aligned components of TXAS. The amino acid side chains of TXAS were then placed on the main chain model, with each side chain conformation set to the most common dihedral angle. The loops between helices were then inserted into the model. These loop conformations were modified using the loop refinement method to optimize a segment of the protein structure. The structure and orientation of the heme in TXAS were adopted directly from the X-ray coordinates of the CYP3A4 heme. Finally, an energy minimization routine with 10^5 steps of the steepest descent was performed for the heme-containing TXAS model causing minor shifts in the position of coordinates to remove steric clashes between atoms and produced a reasonable peptide folding. This allowed the root-mean-square (rms) force to be decreased to −0.5 kcal mol^{-1} Å^{-1}. Profiles-3D and Ramachandran Plot were used to check the validity of the 3D TXAS structure by measuring the compatibility of the simulated TXAS structure with the sequence of TXAS.

dx.doi.org/10.1021/bi301400t | *Biochemistry* 2013, 52, 1113−1121

Molecular Dynamics (MD) Simulations of Clotrimazole and TNS-Docking TXAS. The TNS and clotrimazole structures were generated, optimized, and docked into the pocket of TXAS using the CHARMM-based molecular dynamics docking algorithm. The docking was monitored with a continuous energy calculation, allowing the tracking of the empirical location of the lowest-energy orientation of probes TNS and clotrimazole in the cavity. The flexibility of the probe was addressed by including different orientations of its rotatable side chains in the docking procedure. For analyses of the docked TNS−clotrimazole−TXAS complex, 10^8 conformation structures were generated, among which representatives of the stable conformations were selected on the basis of the energy level of the structures. The numbers of remaining conformations were then minimized by using the docking results with the lowest energy as a starting point for further MD simulations.

RESULTS AND DISCUSSION

Amino Acid Sequence Comparison between TXAS and CYP3A4. The homology of the amino acid sequence between TXAS and other P450 heme protein superfamily members was assessed to select a suitable ligand for the fluorescence probe experiments and structural simulations. The search of amino acid sequence homology by means of comparing TXAS with the nonredundant protein database using the BLAST algorithm revealed that TXAS exhibits its greatest level of homology with CYP3A4 [32.7% identical and 57.2% similar (Figure 1)]. The crystal structure of human CYP3A4 was resolved independently with or without bound ligand.[14,31] Both results showed good structural agreement and revealed a relatively large substrate binding cavity to accommodate either large ligands or multiple smaller ligands for cooperativity. It was also suggested that an unexpected peripheral binding site may be located above the Phe cluster, which may be related to the possible existence of allosteric regulation.[14] When TNS was used as a fluorescent probe to investigate its binding to CYP3A4, it was revealed that TNS indeed bound in the active site and exhibited a concentration-dependent inhibition of CYP3A4 activity.[21] Because of the high degree of sequence similarity between TXAS and CYP3A4, TNS was selected as a probe, and CYP3A4-based structural simulation was employed to characterize the location and topography of the ligand binding site(s) of TXAS.

Fluorescence Probe Experiments. To assess the spatial relationship of ligand binding to TXAS, TNS−TXAS binding dynamics was examined using both steady-state and time-resolved fluorescence spectroscopy, which would provide valuable information about the location of TNS binding. The experiment in which the UV−visible difference spectra were generated by titration of wild-type TXAS with increasing concentrations of TNS (from 0 to 98 μM) showed that addition of TNS did not perturb the immediate environment of the heme iron in TXAS, as evidenced by no apparent changes of the difference spectra around the Soret band (>410 nm) with an increase in TNS concentration (see Figure S1 of the Supporting Information). This is in sharp contrast to a previous observation by Lampe and Atkins, who concluded that TNS bound to the distal heme site of CYP3A4 and thus perturbed the heme spin state of CYP3A4.[21] The absence of the Soret peak shift suggested that there was a lack of direct binding of TNS to the heme iron of TXAS. In addition, the intrinsic protein Trp fluorescence was evaluated to probe the binding site of TNS in TXAS. Upon titration of TXAS with TNS (from 0 to 98 μM), the steady-state Trp fluorescence decreased while emission from TNS increased (Figure 2), indicating a possible energy transfer between TNS and Trp residues or a TNS-induced conformational change of the Trp environment. Using one-site ligand binding fitting (eq 3) of Trp emission from 290 to 375 nm, an apparent dissociation constant (K_d) of 34 ± 5 μM was found (Figure 2). The observation of TNS−Trp interaction and the lack of TNS-induced heme iron spin-state perturbation indicated that TNS is likely to bind in a remote corner of the heme active site or at a distinct peripheral site of TXAS.

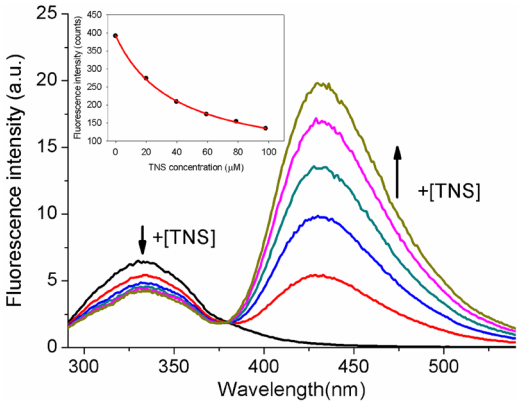

Figure 2. Emission spectra of titration of TXAS (2 μM) with TNS (from 0 to 98 μM) excited at 280 nm. Increasing concentrations of TNS quenched emission from tryptophan but increased emission from TNS. The arrows indicate increasing TNS concentrations. The inset shows the total fluorescence area under the curve from 290 to 375 nm is integrated, and the data are plotted as a function of TNS concentration and fit to eq 3, yielding a K_d of 34 ± 5 μM.

This distinct characteristic for binding of TNS to TXAS was further investigated by the addition of clotrimazole, a well-known high-affinity heme ligand for TXAS.[10] The difference spectral perturbation titration (Figure 3) illustrated the binding of clotrimazole to the TXAS−TNS complex showing a peak at 431 nm and a trough at 412 nm with an apparent K_d of 0.5 ± 0.1 μM as fit with a one-site saturation ligand binding model. The heme iron spin-state perturbation indicated strong binding between clotrimazole and heme in the TXAS−TNS complex. However, the addition of clotrimazole to the TXAS−TNS complex caused negligible changes in the fluorescence intensity or peak of TNS (Figure 3B), illustrating that TNS is not competitively displaced by the binding of clotrimazole. This result was in contrast to that observed for CYP3A4 in which TNS was replaced by erythromycin (ERY)[21] in a similar competitive binding experiment against ERY. This finding further confirmed that TNS does not interact directly with the heme iron in TXAS.

Because TNS could quench emissions from Trp in TXAS, the five Trp residues (Trp31, Trp65, Trp133, Trp203, and Trp446) in TXAS were mutated individually to define the exact Trp residue that is in the proximity of TNS. Five TXAS mutants (W31F, W65F, W133F, W203F, and W446F) were constructed by individually mutating each of all five Trp residues in wild-type TXAS to Phe. The fluorescence emission spectra of Trp residues (excited at 280 nm) were then recorded for the wild type and each mutant TXAS titrated with various concentrations of TNS. The apparent K_d values for binding of

dx.doi.org/10.1021/bi301400t | Biochemistry 2013, 52, 1113−1121

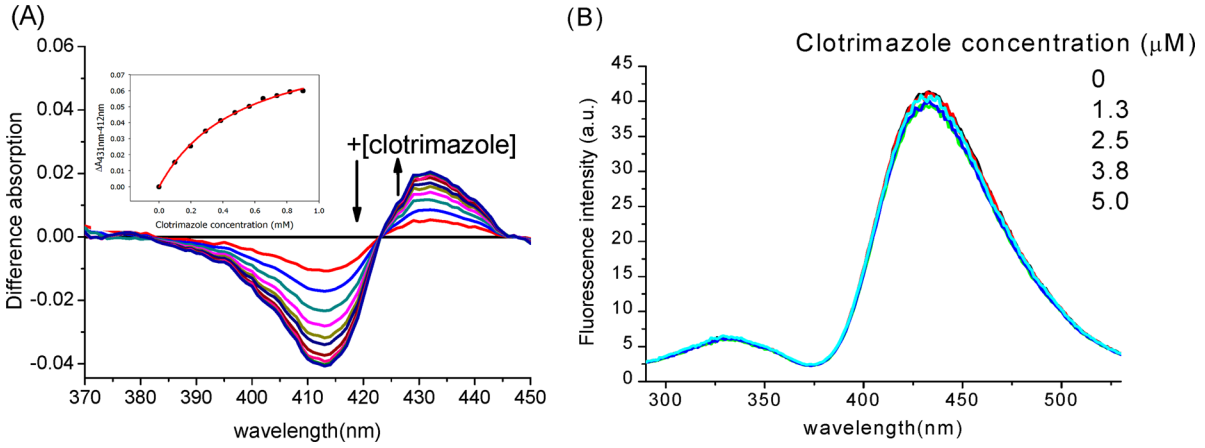

Figure 3. (A) Difference absorption spectra of TNS (56.6 μM)-bound 2 μM TXAS titrated with 0–0.9 μM clotrimazole. The inset shows the absorbance difference between 431 and 412 nm ($\Delta Abs_{431-412}$), among different clotrimazole concentrations that are fit by a one-site saturation ligand binding equation, yielding a K_d of 0.5 ± 0.1 μM. (B) Fluorescence emission spectra of TNS (56.6 μM)-bound TXAS (2 μM) titrated with clotrimazole (from 0 to 5 μM) excited at 280 nm.

TNS to TXAS mutants were not significantly different from each other (25 ± 7 μM for W31F, 15 ± 3 μM for W65F, 27 ± 4 μM for W133F, 42 ± 5 μM for W203F, and 17 ± 4 μM for W446F). The wild type and all TXAS mutants except W65F showed obvious decreases in fluorescence emission intensity integrated from 290 to 375 nm with an increasing TNS concentration (from 0 to 98 μM) compared with that of no TNS control (Figure 4), and none of Trps was quenched

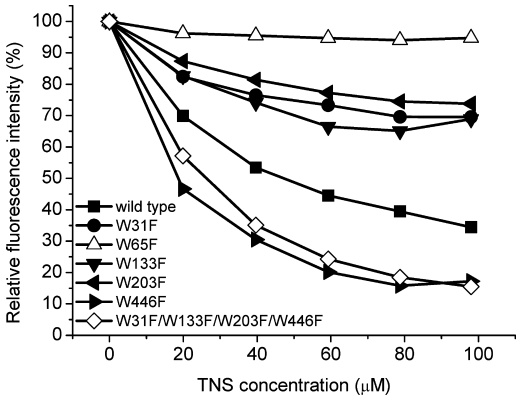

Figure 4. Relative tryptophan emission from 290 to 375 nm of various TXAS Trp mutants (2 μM) titrated with TNS (from 0 to 98 μM) excited at 280 nm. W31F/W133F/W203F/W446F is a quadruple Trp mutant with only W65 preserved. The fluorescence intensity is normalized to the fluorescence emission of respective mutants without addition of TNS.

drastically by either heme or the local microenvironment (the estimated fluorescence intensity ratios for each Trp in TXAS are listed in Table S1 of the Supporting Information), suggesting that Trp65 is the major contributor in energy transfer with TNS. This is further confirmed by using a quadruple Trp mutant (W31F/W133F/W203F/W446F) constructed to test this hypothesis by mutating Trp31, Trp133, Trp203, and Trp446 to Phe, leaving only one Trp, Trp65. When excited at 280 nm, this quadruple mutant exhibited a strong fluorescence quench (~85%) upon addition of 98 μM TNS (Figure 4).

The excited-state decay of TNS bound to TXAS was then analyzed to further probe the spatial relationship between TNS and the Trp residues. There are five Trp residues in TXAS. Therefore, a certain variation in the excited-state relaxation dynamics may be expected. According to previous reports, in a protein, the main difference among each Trp lifetime was primarily due to the polarity and perturbation from neighboring amino acids and the microenvironment around the Trp residues. Interpretations of the complex decay of tryptophan fluorescence are generally classified into two categories, ground-state heterogeneity (e.g., rotamer model) and excited-state reaction (e.g., relaxation model), while the specific origin is still pending resolution. In brief, proteins are heterogeneous systems with various internal motions that cover a wide range of correlation (in time domain), including the nanosecond time window of fluorescence.[32] Nevertheless, in general, tryptophan lifetimes are known to be reduced when exposed to polar environments.[33,34]

As shown in Table 1, we have made attempts to fit two components of each Trp, which has been commonly adopted for the study of tryptophan lifetimes in a protein context.[32] The Trp65 lifetime can be resolved in a straightforward manner in

Table 1. Fluorescence Lifetime Parameters for Tryptophan in TXAS with or without TNS[a]

sample	τ_1 (ns) (α_1)	τ_2 (ns) (α_2)	τ_3 (ns) (α_3)
wild-type TXAS	1.3 (0.17)	3.6 (0.52)	6.1 (0.31)
wild-type TXAS with 50 μM TNS	1.3 (0.22)	3.7 (0.78)	
W31F TXAS	1.1 (0.18)	3.5 (0.52)	6.0 (0.30)
W31F TXAS with 50 μM TNS	1.1 (0.19)	3.6 (0.81)	
W65F TXAS	1.4 (0.31)	3.5 (0.69)	
W65F TXAS with 50 μM TNS	1.2 (0.29)	3.4 (0.71)	
W133F TXAS	1.4 (0.25)	3.7 (0.58)	5.9 (0.17)
W133F TXAS with 50 μM TNS	1.3 (0.12)	3.7 (0.88)	
W203F TXAS	1.1 (0.12)	3.5 (0.74)	5.9 (0.14)
W203F TXAS with 50 μM TNS	1.2 (0.04)	3.5 (0.96)	
W446F TXAS	1.3 (0.18)	3.6 (0.30)	6.0 (0.52)
W446F TXAS with 50 μM TNS	1.3 (0.21)	3.7 (0.79)	
W31F/W133F/W203F/W446F TXAS	1.2 (0.10)		5.9 (0.90)
W31F/W133F/W203F/W446F TXAS with 50 μM TNS	1.2 (0.06)	4.0 (0.94)	

[a]The system response limit is 0.3 ns.

dx.doi.org/10.1021/bi301400t | *Biochemistry* 2013, 52, 1113–1121

W31F/W133F/W203F/W446F TXAS without TNS (1.2 ns, 5.9 ns, χ^2 = 1.1) and with 50 μM TNS (1.2 ns, 4.0 ns, χ^2 = 1.2). While the short decay component remains nearly unchanged, the decrease in the decay time from 5.9 to 4.0 ns is obvious, which implies an efficient energy transfer between Trp65 and TNS (vide infra). In yet another approach, the fluorescence lifetimes of the other four Trp residues (Trp31, Trp133, Trp203, and Trp446) were measured in W65F TXAS. We started the fitting from the assumption of four distinct lifetimes for four Trp residues s for the long decay component ranging from 3.0 to 6.0 ns. In this approach, similar to that of Trp65 in W31F/W133F/W203F/W446F TXAS, we assumed that the ~1 ns short decay component remained unchanged among all Trp residues because of its short life span and hence less quenching by any other processes. In other words, only one variable was used to fit the short decay component, but four variables were applied for the long decay component during the fitting process. As a result, the best fit gave four very close long decay component, which was considered to be virtually irresolvable if we took into account the uncertainty of error. In yet another approach, upon using only one decay rate constant to fit the long decay component, we obtained lifetimes of 1.4 and 3.5 ns for short and long decay components, respectively, with a statistical confidence factor (χ^2) of 1.2. The latter value is very close to an average of four individual fitted decay constants. Therefore, except for Trp65 ($\tau \sim$ 5.9 ns), which is expected to have the longest fluorescence lifetime because of its proximity to the more nonpolar and/or hydrophobic environment, we concluded that the other four Trp residues are in a similar polar and/or proximal amino acid environment, as indicated by the fluorescence lifetime of ~3.5 ns. Furthermore, the longer lifetime of Trp65 can be distinctly separated from those of the other four Trp residues. This is further supported by the fitting of W31F TXAS, W133F TXAS, W203F TXAS, W446F TXAS, and even wild-type TXAS, the results of which always show a separable, long decay component of 5.9–6.1 ns that can reasonably be ascribed to the fluorescence lifetime of Trp65 (Table 1).

Along the same line, we further performed the TNS titration and obtained Trp decay times for W65F TXAS of 1.2 and 3.4 ns for short and long decay components, respectively, upon addition of 50 μM TNS (the same concentration used for titration of W31F/W133F/W203F/W446F TXAS). The reduction in lifetime from 3.5 to 3.4 ns indicated only minimal quenching via the energy transfer process by the other four Trp residues. This, together with the TXAS homology model, yielded Trp distances listed in a later section, leads us to conclude that there is no obvious energy transfer between TNS and the other four Trp residues. As described in the computational section below, the inefficient energy transfer process is plausibly caused by the combination of two factors: longer TNS–Trp distance and shorter Trp fluorescence lifetime (3.5 ns vs 5.9 ns for Trp65). As a result, thereafter, we focused on Trp65 because of its distinctly short distance toward TNS and hydrophobic environment (vide infra).

On the basis of the mechanism of Förster resonance energy transfer, the Förster distance (R_0) of energy transfer between TNS and Trp was calculated to be 25 Å (eq 6). Accordingly, the distance (r) between TNS and Trp65 (point center) was deduced to be 19 Å. Details of the relevant calculation are provided in the Supporting Information. Note that the observed variation in the fluorescence intensity decay ratio (Figure 4) and in the decrease in the lifetime of wild-type and mutant TXAS (Table 1) was primarily due to the perturbation from neighboring amino acids and the microenvironment around each Trp residue. For example, to a certain extent, amino acids such as aspartate, glutamate, lysine, and arginine may slightly quench Trp fluorescence.[32]

Additionally, Nile Red, a hydrophobic dye sensitive to environmental polarity,[35] was utilized to investigate competitiveness and the microenvironment of the TNS binding site in TXAS. Titration of TXAS with Nile Red resulted in the enhancement of emission at 632 nm, which occurred in a concentration-dependent manner with an apparent K_d of 2.7 ± 0.3 μM by fitting to a one-site ligand saturation binding model (Figure 5). In contrast to the effect of clotrimazole, the addition

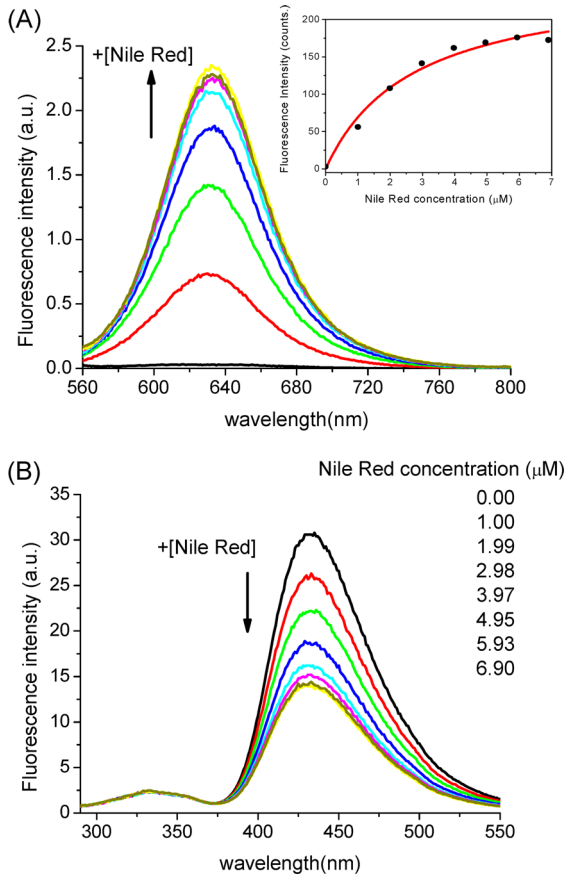

Figure 5. (A) Emission spectra of TXAS (2 μM) titrated with Nile Red (from 0 to 6.9 μM) excited at 550 nm. Increasing concentrations of Nile Red enhance the emission of Nile Red. The arrows indicate increasing Nile Red concentrations. The inset shows the total fluorescence area under the curve from 560 to 800 nm is integrated, and the data are plotted as function of Nile Red concentration and fit by the one-site saturation ligand binding equation, yielding a K_d of 2.7 ± 0.3 μM. (B) Fluorescence emission spectra of TNS (56.6 μM)-bound TXAS (2 μM) titrated with Nile Red (from 0 to 6.9 μM) excited at 280 nm.

of Nile Red to the TXAS–TNS complex decreased the fluorescence intensity of TNS (Figure 5B). However, the fluorescence lifetime of TNS in TXAS did not change in the absence (1.8 ns) or presence (1.7 ns) of 6.9 μM Nile Red. This indicated that there is no obvious energy transfer between TNS and Nile Red. Thus, TNS is most likely to be competitively displaced by the binding of Nile Red to TXAS. In other words, upon competitive replacement with Nile Red, TNS is ejected

dx.doi.org/10.1021/bi301400t | Biochemistry 2013, 52, 1113–1121

from TXAS to the solution. This is further supported by the fact that TNS fluoresces very weakly in aqueous solution in the region of ~500 nm. Because Nile Red is known to exhibit a high emission yield when located in a hydrophobic environment, these results imply that the TNS binding site in TXAS, which is in the proximity of Trp65, is likely to be hydrophobic.

TXAS Structure and Probing the Heme Active Site with TNS. On the basis of the MD simulations, the distance measurements between Trps and TNS in TXAS are illustrated in Figure 6A. The measurements show that Trp65 is the closest to TNS at a distance of ~14 Å compared to the other four Trp residues (Trp31, Trp133, Trp203, and Trp446), with distances of >25 Å. As shown in Figure 6B, our comprehensive docking simulations suggest that the binding sites for clotrimazole and TNS, localized to the solvent-accessible surfaces of the substrate access channel extending toward the heme active site, in TXAS are not mutually exclusive. This indicates that TNS binds to a remote corner of the heme pocket, as in the case of testosterone binding in CYP3A4.[14]

To characterize the ligand binding site, the probing molecules, TNS (blue) and clotrimazole (purple), along with relevant encompassing residues in the heme pocket of TXAS are presented in panels B and C of Figure 6. The common core of the heme pocket consists of helix I and the B−C loop connecting helices B and C, which include residues N110, R111, W133, R137, F337, R410, R413, and R478. The hydrophobic binding site of TNS consists of part of helix A, the F−F′ loop, and helices F and G. The residues forming this hydrophobic pocket include N349, F217, F218, E219, F220, F409, F64, and W65; among them, N349 and E219 anchor TNS tightly, as shown in Figure 6C. It is also noteworthy that such a Phe cluster is reminiscent of that was observed and reported for human CYP3A4 in the literature.[14] Moreover, this Phe cluster packing above the heme active site cavity may form a less polar, water-deficient microenvironment. Trp65 is observed to be involved in this hydrophobic pocket; in contrast, residues Trp31, Trp203, and Trp446 are located on the water accessible protein surface, and Trp133 interacts with the heme peripheral propionate matrix (Figure 6A).[36] Apparently, Trp65 is located in a less polar environment compared to the other four Trp residues in TXAS.

Overall, the TXAS active site is much more open in the vicinity of heme, and the cavity volume is more uniformly distributed than the sinuous cavity of its counterenzyme prostacyclin synthase (PGIS) (PDB entry 2IAG).[37] Compared with that of PGIS, the larger volume of the active site around the heme vicinity of TXAS reflects more flexibility in ligand(s) binding at the distal site of heme. Thus, we speculate that this adaptive active site in TXAS might be capable of binding multiple ligands simultaneously because of its large size and flexibility.

CONCLUSION

In summary, using TNS as a fluorescence probe, the proximity between TNS and each of the five tryptophan residues in TXAS was examined through the FRET process. Together with the mutation of TXAS at five individual Trp sites, the results showed that Trp65 is the major contributor to account for energy transfer with TNS, implying that TNS is in the proximity of Trp65. The distance between TNS and Trp65 is estimated to be 19 Å. As for the location of TNS, competitive binding experiments using clotrimazole reveal that, in contrast to CYP3A4, heme and TNS do not interact with each other in

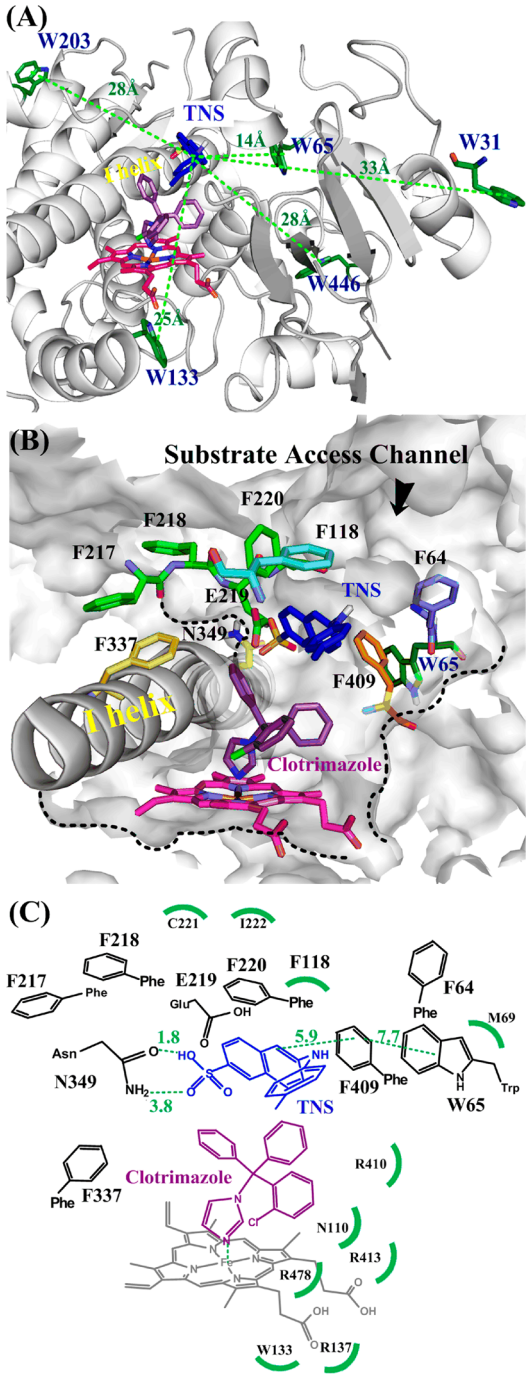

Figure 6. Structures of TNS- and clotrimazole-bound TXAS. (A) The relevant Trp residues, W31, W65, W133, W203, and W446, are shown with center-to-center distance measurements for TNS (in angstroms). (B) Illustration of the solvent access channels that connect the heme active site to the protein surface. The channel edges are outlined by the black dashed lines. Two different ligands, TNS (blue) and clotrimazole (purple), docking in TXAS and related Phe residues in the pocket. (C) Probing molecules, TNS (blue) and clotrimazole (purple), along with relevant encompassing residues in the heme pocket of TXAS (in angstroms).

TXAS. On the contrary, TNS is displaced by Nile Red, a hydrophobic dye sensitive to environmental polarity, indicating that the TNS binding site in TXAS is likely to be a hydrophobic pocket. The result in combination with a computer simulation experiment leads us to conclude that TXAS, like CYP3A4,

dx.doi.org/10.1021/bi301400t | Biochemistry 2013, 52, 1113−1121

possesses a large active site, which can accommodate TNS and clotrimazole without mutual interaction between TNS and heme. The Phe cluster packing near the binding site of TNS may be involved in facilitating the binding of multiple ligands to the large active site of TXAS.

■ ASSOCIATED CONTENT

Supporting Information

Difference absorption spectra of TXAS titrated with TNS and details of the Förster distance calculations. This material is available free of charge via the Internet at http://pubs.acs.org.

■ AUTHOR INFORMATION

Corresponding Author

*School of Medicine, Fu-Jen Catholic University, 510 Zhongzheng Rd., Xinzhuang District, New Taipei City 24205, Taiwan, R. O. C. Telephone: 886-2-29053406. Fax: 886-2-29052095. E-mail: 034407@mail.fju.edu.tw.

Notes

The authors declare no competing financial interest.

■ ABBREVIATIONS

TXAS, thromboxane A_2 synthase; CYP3A4, cytochrome P450 3A4; PGH_2, prostaglandins H_2; TXA_2, thromboxane A_2; TNS, 2-*p*-toluidinylnaphthalene-6-sulfonic acid; HHT, 12-L-hydroxy-5,8,10-heptadecatrienoic acid; MDA, malondialdehyde; *δ*-ALA, *δ*-aminolevulinic acid.

■ REFERENCES

(1) Hecker, M., and Ullrich, V. (1989) On the mechanism of prostacyclin and thromboxane A_2 biosynthesis. *J. Biol. Chem. 264*, 141−150.

(2) Samuelsson, B., Goldyne, M., Granstrom, E., Hamberg, M., Hammarstrom, S., and Malmsten, C. (1978) Prostaglandins and thromboxanes. *Annu. Rev. Biochem. 47*, 997−1029.

(3) Needleman, P., Turk, J., Jakschik, B. A., Morrison, A. R., and Lefkowith, J. B. (1986) Arachidonic acid metabolism. *Annu. Rev. Biochem. 55*, 69−102.

(4) Ogletree, M. L. (1987) Overview of physiological and pathophysiological effects of thromboxane A_2. *Fed. Proc. 46*, 133−138.

(5) Hamberg, M., Svensson, J., and Samuelsson, B. (1975) Thromboxanes: A new group of biologically active compounds derived from prostaglandin endoperoxides. *Proc. Natl. Acad. Sci. U.S.A. 72*, 2994−2998.

(6) Uchida, K. (1999) Current status of acrolein as a lipid peroxidation product. *Trends Cardiovasc. Med. 9*, 109−113.

(7) Chaudhary, A. K., Nokubo, M., Reddy, G. R., Yeola, S. N., Morrow, J. D., Blair, I. A., and Marnett, L. J. (1994) Detection of endogenous malondialdehyde-deoxyguanosine adducts in human liver. *Science 265*, 1580−1582.

(8) Yokoyama, C., Miyata, A., Ihara, H., Ullrich, V., and Tanabe, T. (1991) Molecular cloning of human platelet thromboxane A synthase. *Biochem. Biophys. Res. Commun. 178*, 1479−1484.

(9) Ohashi, K., Ruan, K. H., Kulmacz, R. J., Wu, K. K., and Wang, L. H. (1992) Primary structure of human thromboxane synthase determined from the cDNA sequence. *J. Biol. Chem. 267*, 789−793.

(10) Hsu, P. Y., Tsai, A. L., Kulmacz, R. J., and Wang, L. H. (1999) Expression, purification, and spectroscopic characterization of human thromboxane synthase. *J. Biol. Chem. 274*, 762−769.

(11) Haurand, M., and Ullrich, V. (1985) Isolation and characterization of thromboxane synthase from human platelets as a cytochrome P-450 enzyme. *J. Biol. Chem. 260*, 15059−15067.

(12) Ruan, K. H., Milfeld, K., Kulmacz, R. J., and Wu, K. K. (1994) Comparison of the construction of a 3-D model for human thromboxane synthase using P450cam and BM-3 as templates: Implications for the substrate binding pocket. *Protein Eng. 7*, 1345−1351.

(13) Wang, L. H., Matijevic-Aleksic, N., Hsu, P. Y., Ruan, K. H., Wu, K. K., and Kulmacz, R. J. (1996) Identification of thromboxane A_2 synthase active site residues by molecular modeling-guided site-directed mutagenesis. *J. Biol. Chem. 271*, 19970−19975.

(14) Williams, P. A., Cosme, J., Vinkovic, D. M., Ward, A., Angove, H. C., Day, P. J., Vonrhein, C., Tickle, I. J., and Jhoti, H. (2004) Crystal structures of human cytochrome P450 3A4 bound to metyrapone and progesterone. *Science 305*, 683−686.

(15) Scott, E. E., and Halpert, J. R. (2005) Structures of cytochrome P450 3A4. *Trends Biochem. Sci. 30*, 5−7.

(16) Lehrer, S. S. (1971) Solute perturbation of protein fluorescence. The quenching of the tryptophyl fluorescence of model compounds and of lysozyme by iodide ion. *Biochemistry 10*, 3254−3263.

(17) Eftink, M. R., and Ghiron, C. A. (1981) Fluorescence quenching studies with proteins. *Anal. Biochem. 114*, 199−227.

(18) Narasimhulu, S. (1988) Quenching of tryptophanyl fluorescence of bovine adrenal P-450C-21 and inhibition of substrate binding by acrylamide. *Biochemistry 27*, 1147−1153.

(19) Lange, R., Anzenbacher, P., Muller, S., Maurin, L., and Balny, C. (1994) Interaction of tryptophan residues of cytochrome P450scc with a highly specific fluorescence quencher, a substrate analogue, compared to acrylamide and iodide. *Eur. J. Biochem. 226*, 963−970.

(20) Brand, L., and Gohlke, J. R. (1972) Fluorescence probes for structure. *Annu. Rev. Biochem. 41*, 843−868.

(21) Lampe, J. N., and Atkins, W. M. (2006) Time-resolved fluorescence studies of heterotropic ligand binding to cytochrome P450 3A4. *Biochemistry 45*, 12204−12215.

(22) Albani, J. R. (2009) Fluorescence origin of 6,P-toluidinyl-naphthalene-2-sulfonate (TNS) bound to proteins. *J. Fluoresc. 19*, 399−408.

(23) Nath, A., Grinkova, Y. V., Sligar, S. G., and Atkins, W. M. (2007) Ligand binding to cytochrome P450 3A4 in phospholipid bilayer nanodiscs: The effect of model membranes. *J. Biol. Chem. 282*, 28309−28320.

(24) Lakowicz, J. R. (2006) *Principles of Fluorescence Spectroscopy*, 3rd ed., Springer, New York.

(25) Hsu, P. Y., and Wang, L. H. (2003) Protein engineering of thromboxane synthase: Conversion of membrane-bound to soluble form. *Arch. Biochem. Biophys. 416*, 38−46.

(26) Lakowicz, J. R. (1999) *Principles of fluorescence spectroscopy*, 2nd ed., Kluwer Academic/Plenum, New York.

(27) Chou, P.-T., Chen, Y.-C., Yu, W.-S., Chou, Y.-H., Wei, C.-Y., and Cheng, Y.-M. (2001) Excited-State Intramolecular Proton Transfer in 10-Hydroxybenzo[h]quinoline. *J. Phys. Chem. A 105*, 1731−1740.

(28) Clapp, A. R., Medintz, I. L., Mauro, J. M., Fisher, B. R., Bawendi, M. G., and Mattoussi, H. (2004) Fluorescence Resonance Energy Transfer Between Quantum Dot Donors and Dye-Labeled Protein Acceptors. *J. Am. Chem. Soc. 126*, 301−310.

(29) Suzukida, M., Le, H. P., Shahid, F., McPherson, R. A., Birnbaum, E. R., and Darnall, D. W. (1983) Resonance energy transfer between cysteine-34 and tryptophan-214 in human serum albumin. Distance measurements as a function of pH. *Biochemistry 22*, 2415−2420.

(30) Wang, Z. J., Ren, L. X., Zhao, Y. Q., Li, G. T., Duan, L., Liang, A. H., and Yang, B. S. (2008) Investigation on the binding of TNS to centrin, an EF-hand protein. *Spectrochim. Acta, Part A 70*, 892−897.

(31) Yano, J. K., Wester, M. R., Schoch, G. A., Griffin, K. J., Stout, C. D., and Johnson, E. F. (2004) The structure of human microsomal cytochrome P450 3A4 determined by X-ray crystallography to 2.05-Å resolution. *J. Biol. Chem. 279*, 38091−38094.

(32) Ladokhin, A. S. (2006) Fluorescence Spectroscopy in Peptide and Protein Analysis. In *Encyclopedia of Analytical Chemistry*, John Wiley & Sons, Ltd., New York.

(33) Chattopadhyay, A., Rawat, S. S., Kelkar, D. A., Ray, S., and Chakrabarti, A. (2003) Organization and dynamics of tryptophan residues in erythroid spectrin: Novel structural features of denatured

spectrin revealed by the wavelength-selective fluorescence approach. *Protein Sci. 12*, 2389−2403.
(34) Huggins, K. W., Curtiss, L. K., Gebre, A. K., and Parks, J. S. (1998) Effect of long chain polyunsaturated fatty acids in the sn-2 position of phosphatidylcholine on the interaction with recombinant high density lipoprotein apolipoprotein A-I. *J. Lipid Res. 39*, 2423−2431.
(35) Sackett, D. L., and Wolff, J. (1987) Nile red as a polarity-sensitive fluorescent probe of hydrophobic protein surfaces. *Anal. Biochem. 167*, 228−234.
(36) Hsu, P. Y., Tsai, A. L., and Wang, L. H. (2000) Identification of Thromboxane Synthase Amino Acid Residues Involved in Heme-Propionate Binding. *Arch. Biochem. Biophys. 383*, 119−127.
(37) Chiang, C. W., Yeh, H. C., Wang, L. H., and Chan, N. L. (2006) Crystal structure of the human prostacyclin synthase. *J. Mol. Biol. 364*, 266−274.